DOI: 10.1002/fuce.200500212

Transient Analysis of Proton Electrolyte Membrane Fuel Cells (PEMFC) at Start-Up and Failure

M. F. Serincan[1], and S. Yesilyurt[1]*

[1] Sabanci University, Tuzla 34956, Istanbul, Turkey

Received July 1, 2005; accepted May 23, 2006

Abstract

A two-dimensional, transient, single-phase computational model, incorporating water transport in the membrane and the flow and transport of species in porous gas diffusion electrodes is developed to evaluate the transient performance of a PEMFC with interdigitated gas distributors. The co-flow and counter-flow of the anode and cathode reactants are discussed to address their effects on PEMFC performance and transients. The important role of water transport in the membrane on the transients is demonstrated. The membrane's water intake or outtake determines the duration of the transients. The effect of the operating conditions on steady state and transient performances is outlined. Overshoots and undershoots are observed in the average current density, due to a step change in the cell voltage and the cathode pressure under start-up conditions. Simulation results are used to address the role of auxiliary components in the failure modes of the PEMFC.

Keywords: CFD, Gas Diffusion Electrode, Membrane, PEMFC, Water Transport

1 Introduction

In a PEMFC with conventional flow fields, the reactants are mainly transported to catalyst sites by diffusion, which often leads to mass transfer limitations. The enhanced performance of the fuel cell has already been reported, when interdigitated flow fields are used [1]. In this flow field design, dead ended gas channels grooved on the current collector plates force reactant gases to flow through porous anode and cathode electrodes, resulting in convection dominated mass transport. Forced flow in the electrodes helps the reactants to reach the catalyst sites faster, and liquid water is dragged out of the system by this flow and by evaporation [2]. In a study comparing the two flow field designs, Kazim et al. [3] asserted that interdigitated flow fields help to cause the limiting current density to increase up to three times and the maximum power density to increase two folds [3].

Modeling a PEMFC with interdigitated gas distributors and porous electrodes is somewhat different than modeling a PEMFC with conventional, serpentine gas distributors and gas diffusion layers. Research reports that address modeling issues for the interdigitated flow fields and that compare the two designs exist. Kazim et al. developed a two-dimensional model of reactant transport in the cathode to compare conventional and interdigitated gas distributor designs, and demonstrated that interdigitated design allows higher power densities than the conventional distributors [3]. Modeling mass transport in the cathode of an interdigitated PEMFC, Yi and Nguyen concluded that current density improves with increasing rate of reactant flow in the electrodes, as a result of the pressure difference applied between the inlet and outlet channels [4]. Wang and Liu [5] developed a 3D steady-state model to conduct parametric studies on PEMFCs, along with experiments to study the effect of temperature, humidity, and pressure on fuel cell performance. They concluded that as long as the cell is well humidified, increasing the temperature and pressure always improves cell performance. Hu et al. [6, 7] developed a 3D, two-phase, steady-state model where both of the boundary conditions for conventional and interdigitated flow fields can be implemented. According to their results, the interdigitated design performs poorly without cathode humidification, compared to the conventional design. Furthermore, the authors conclude that the shear force of the flow removes the liquid water from the porous

[*] *Corresponding author, syesilyurt@sabanciuniv.edu*

cathode electrode, and that single phase flow conditions are present in the porous cathode. He et al. reported the drag effect of the gas flow in removing liquid water from the cathode porous electrode. In addition to evaporation, in their study a 2D, two-phase, steady-state flow model was used for the cathode of a PEMFC with interdigitated gas distributors [8].

Generally speaking, the transients experienced by a fuel cell are among the major factors affecting the system performance and lifetime. In many applications, transients, especially during the start-up of the system, are significant in terms of the lifetime of a PEMFC. PEMFC transient modeling gives important perspectives relating to design, operation, control and maintenance of the system. A recent study of PEMFC dynamics by Benziger et al. [9] readily demonstrates that PEMFCs have strong nonlinear behavior and may show long-period steady oscillations associated with the membrane water uptake. Kim et al. [10] showed that PEMFCs may exhibit a second-order dynamic behavior, and, hence, sharp overshoots and undershoots. The authors concluded that the flow field design is of the utmost importance in fuel cell transients. Finally, Friede et al. [11] developed a one-dimensional mathematical model to characterize the transient behavior of a PEMFC, they concluded that the membrane water transport has a very strong influence on the fuel cell transients. A recent study by Wang and Wang [12] demonstrates that the effect of water transport in the membrane is characterized by a time-scale in the range of 10 s, whereas the charging and discharging of the electrochemical layer is negligibly fast.

This work aims to develop a two-dimensional transient transport and water management model, for an interdigitated PEMFC membrane electrode assembly. The objective is to study the effect of step changes in cell voltage, cathode air pressure, and relative humidity during start-ups and failures of auxiliary components, such as the loss of pressure in the case of compressor or manifold malfunctions and the loss of humidity in the case of a humidifier malfunction.

2 Model Definition

The model presented here is a two-dimensional transient model of coupled transport processes in the gas diffusion electrodes, catalyst layers, and the membrane. It is considered that water exists only in the gas phase at the electrodes, and as solute water in the membrane. The cell temperature is assumed to be constant. The catalyst layers are assumed to be very thin and are considered as reactive surfaces not volumes.

This model covers both co-flow and counter-flow designs. In an interdigitated PEMFC with a gas distributor, as sketched in Figure 1, there are two different configurations. These are: (i) where the anode and cathode flow channels, facing each other across the membrane, have the same direction from inlet to outlet, this design is called co-flow; (ii) where the inlet of the anode (cathode) is facing the outlet

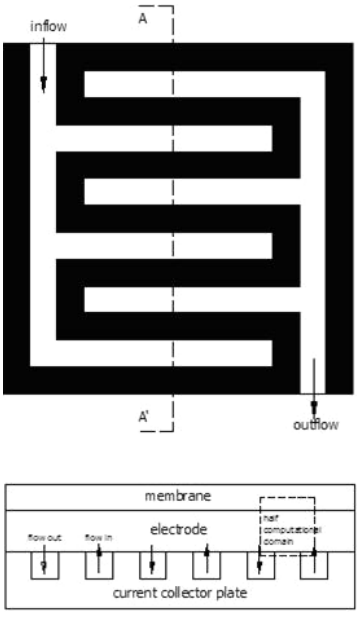

Fig. 1 Top view of an interdigitated gas distributor (top), and A-A' cross-section of the half-cell (bottom); the region enclosed with dashed lines is half of the computational domain.

of the cathode (anode) across the membrane, this configuration is called counter-flow.

The single-phase model described here is sufficient for the modeling of flow in a porous anode and cathode over a range of current densities and humidity conditions at the cathode. As previously reported [6–8], the forced flow conditions ensure single-phase conditions up to moderately high current densities. Severe flooding of the cathode, where the concentration losses become significant, only occurs at very high current densities. Hence, as long as the time-scale associated with the transport of gases in the electrode is suitably small (0.1–1 s according to [12]) compared to the time-scale of

Table 1 Parameters used in the model.

Parameter	Symbol	Value	Unit	Reference
Hydraulic permeability	k_p	1.2×10^{-12}	m^2	[8]
Viscosity of gas	μ	2.03×10^{-5}	kg m^{-1} s^{-1}	[8]
Dry porosity of electrode	ε_g	0.3		[17]
Universal gas constant	R	8.3143	J mol^{-1} K^{-1}	
Conductivity of electrode	σ	727	S m^{-1}	[18]
Conductive portion of electrode	ε_s	0.3		[19]
Dry density of membrane	ρ_m	1,980	kg m^{-3}	[20]
Equivalent weight of membrane	M_m	1.1	kg mol^{-1}	[20]
Faraday's constant	F	96,487	C mol^{-1}	
Water mass transfer coefficient	γ	1.14×10^{-4}	m s^{-1}	estimated
Asymmetry parameter	β	0.5		[21]
Cathode transfer coefficient	k	0.5		[8]
Exchange current density	$I_{0,c}$	700	A m^{-2}	estimated
Anode current constant	k_a	17×10^7		[21]
Concentration parameter	γ_{H2}	0.25		[22]
Water fraction in membrane	ε_m	0.26		[12]

membrane water transport (about 10 s), it is sufficient to use a single-phase model for this study.

2.1 Governing Equations

2.1.1 Gas Diffusion Electrodes

The flow in porous gas diffusion electrodes can be determined from Darcy's Law, which states that the flow velocity, **u**, is proportional to the pressure gradient within the porous medium. The proportionality constant is given by the ratio of the permeability, k_p, of the porous medium and the viscosity of the fluid, μ:

$$\mathbf{u} = -\frac{k_p}{\mu}\nabla p. \tag{1}$$

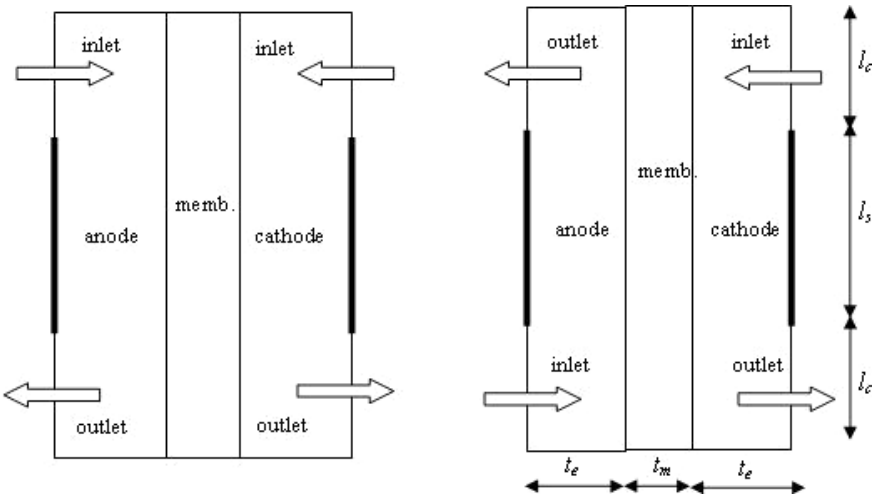

Fig. 2 Computational domain and dimensions of the fuel cell for co-flow (a) and counter-flow (b).

The velocity of the fluid is subject to the condition:

$$\frac{\partial}{\partial t}(\rho\varepsilon_g) + \nabla.(\rho\varepsilon_g\mathbf{u}) = 0, \tag{2}$$

where ε_g is the dry porosity of the electrode.

The transport of each species in the gas diffusion electrodes is governed by the Maxwell-Stefan equation, in the form developed by Curtiss and Bird [14]. This is more suitable than Fick's Law of binary diffusion for the case of interdiffusion of species and multi component transport [15]:

$$\frac{\partial}{\partial t}(\rho\varepsilon_g w_i) + \nabla.\left[-\rho w_i \sum_{j=1}^{N} D_{ij}\left\{\left(\nabla x_j + \left(x_j - w_j\right)\frac{\nabla p}{p}\right)\right\} + \rho w_i \mathbf{u}\right] = 0 \tag{3}$$

The model takes two species in the anode, H_2 and H_2O, and three species in the cathode, O_2, H_2O, and N_2, into account. Eq. (3) is used for H_2 at the anode, and for O_2 and H_2O at the cathode. Since the sum of the mass fractions in the domain is unity, the mass fractions of H_2O at the anode and N_2 at the cathode are given in terms of the mass fractions of other gases. In the Maxwell-Stefan equation, the density of the mixture, ρ, is given by

$$\frac{1}{\rho} = \frac{\sum_i \frac{w_i}{M_i}}{p/(R.T)}. \tag{4}$$

The binary diffusion coefficients, which characterize the interactions between a pair of species, can be determined at an arbitrary temperature and pressure from [16],

$$D_{ij} = D_{ij}^0(p_0, T_0)\frac{p_0}{p}\left(\frac{T}{T_0}\right)^{1.5} \tag{5}$$

The nominal values at reference temperatures and pressures are listed in Table 2. To account for the porosity, the effective diffusion coefficient is calculated with a Bruggeman type relation, [16],

Table 2 Binary diffusivities at reference temperatures and 1 atm [4].

Gas pair	Reference temperature T_0 / K	Binary diffusivity constant / $m^2\ s^{-1}$
$H_2 - H_2O$	307.1	0.915×10^{-4}
$O_2 - H_2O$	308.1	0.282×10^{-4}
$O_2 - N_2$	293.2	0.220×10^{-4}
$H_2O - N_2$	307.5	0.256×10^{-4}

$$D_{ij}^{eff} = D_{ij}\varepsilon_g^{1.5}. \tag{6}$$

Ohm's Law is used for charge conservation in the conductive electrodes:

$$\nabla.(\sigma^{eff}\nabla\varphi) = 0 \tag{7}$$

Only the solid phase of the electrodes are conductive, thus an effective conductivity is used, which is defined as,

$$\sigma^{eff} = \sigma\varepsilon_s^{1.5}, \tag{8}$$

where ε_s is the volume fraction of electronically conductive solid in the electrodes.

2.1.2 Membrane

In addition to ion transport in the membrane, the transport of water, which carries the utmost importance in transients, is modeled here. There are two distinct mechanisms that govern the transport of water in the membrane [17, 23, 24]: (i) electro-osmotic drag, due to the transport of protons from the anode to cathode; (ii) diffusion, due to the concentration gradient inside the membrane. Most models in the literature impose an equilibrium water sorption value, a function of water activity, as the boundary condition for the membrane's water content [4, 12, 24]. However, water exists in the liquid phase in the membrane, whereas it is assumed to exist in the vapor phase in the electrodes. Thus, as suggested by Berg et

al. [17], a two mode water transfer mechanism is used to incorporate the phase change of water in the membrane, assuming that the flux in and out of the membrane is proportional to the difference between the local water content and the equilibrium sorption value (the proportionality constant is the mass transfer coefficient). Similar assumptions are also commonly used for the membrane-catalyst layer boundary condition, e.g. [25].

Based on the formulation developed by Berg et al. [17], the total mass flux of water transported inside the membrane is given by,

$$\mathbf{J}_w^T = \mathbf{J}_w + \mathbf{J}_+ = -m.D_w \nabla c_w + n_d \frac{\mathbf{I}}{F} \tag{9}$$

where c_w is the normalized molar fraction of water in the membrane with respect to the total concentration of sulfonic acid groups m is the molar concentration of sulfonic acid group, and defined as $m = \rho_{\mathrm{mem}}/M_{\mathrm{mem}}$, where ρ_{mem} is the density of the dry membrane and M_{mem} is the molecular weight of the dry membrane, D_{w} is the diffusivity of water in the solid phase of the membrane, and n_{d} is the number of H_2O molecules dragged by each proton as a function of the water content, c_{w}. Expressions and values for these parameters for a Nafion® membrane are given in Table 3.

In Eq. (9), the term $\mathbf{J}_w$ represents the so called back-diffusion of water in the membrane and the next term, $\mathbf{J}_+$, stands for the water's flux, due to electro-osmotic drag, induced by the ionic current, $\mathbf{I}$. In the model developed here, the conservation of mass is imposed for water as follows:

$$\frac{\partial}{\partial t}(\varepsilon_m.m.c_w) + \nabla.\mathbf{J}_w^T = 0 \tag{10}$$

where ε_{m} is the fraction of water in the membrane per sulfonic group in the solid phase of the membrane. The time-dependent first term in (10) is for the reservoir effect of the membrane.

The conduction of protons in the membrane is modeled using Ohm's Law for the conservation of charge:

$$\nabla.(-\kappa \nabla \varphi) = 0. \tag{11}$$

The capacitive effect of the membrane, which introduces a very fast transient, is neglected here. Note that, the ionic conductivity, κ, of the membrane is dependent on the water content, via a well-known equation for Nafion-type membranes, as given in Table 3.

Table 3 Terms dependent on membrane water content.

Parameter	Expression	Reference
D_{w}	$3.5 \times 10^{-7} \exp(-2436/T)\ c_{\mathrm{w}}$ / $\mathrm{m^2\ s^{-1}}$	[26]
n_{d}	$0.0029\ c_{\mathrm{w}}^2 + 0.05\ c_{\mathrm{w}}$	[27]
κ	$\exp(1268(1/303\text{-}1/T))\ (0.5139\ c_w - 0.326)$ / $\mathrm{S\ m^{-1}}$	[24]

2.2 Boundary Conditions

The boundary conditions used in the model for counter-flow are summarized in Figure 3. Whenever a flux condition is used in the model, it is considered as an inward flux and denoted with a minus sign in front of the normal vectors, as shown in Figure 3. The co-flow and counter-flow cases are distinguished by the anode inlet and outlet boundary conditions. The anode inlet boundary condition for counter-flow is the outlet boundary condition for the co-flow and vice versa.

2.2.1 Electrode Inlets and Outlets

Mole fractions of H_2, H_2O, and O_2 are prescribed for the electrode inlets. Whereas, for the outlets, the corresponding boundary conditions are set to convective flux, which ensures that any mass transport through that boundary is convection dominated and there is no mass flux due to diffusion since the normal component of the fluxes to zero. Inlet and outlet thermodynamic pressures are set for Darcy's Law. Zero-flux boundary conditions are used for Ohm's Law at these boundaries to represent electrical insulation.

2.2.2 Electrode Membrane Interfaces

Flux boundary conditions are used for all the equations at the interface between the electrodes and the membrane. The mass fluxes that appear in the boundary conditions of both the Maxwell-Stefan equation and Darcy's Law are described as,

$$N_{H_2} = \frac{i_a}{2F} M_{H_2} \tag{12}$$

$$N_{H_2O}^a = a \frac{i_a}{F} M_{H_2O} \tag{13}$$

$$N_{O_2} = \frac{i_c}{4F} M_{O_2} \tag{14}$$

$$N_{H_2O}^c = -(2a+1) \frac{i_c}{2F} \tag{15}$$

In Eqs. (12)-(15), a stands for the total water drag from the anode to the cathode, which is defined as

$$a = F \frac{J_w^T}{i_{a,c}(y)}, \tag{16}$$

where $i_{\mathrm{a,c}}(y)$ is the local current density at the anode and the cathode-side, represented by the subscripts 'a' and 'c' respectively, boundaries, where the total water flux is defined in Eq. (9).

For the conservation of charge, the transfer current densities are used to define flux boundary conditions, which are obtained from the Butler-Volmer equation [28]

$$i_{a,c} = i_0 \left(\exp\left(\frac{\beta.n.F}{R.T} \eta \right) - \exp\left(-\frac{(1-\beta).n.F}{R.T} \eta \right) \right), \tag{17}$$

where i_0 is the exchange current density, β is an asymmetry parameter, n is the number of electrons per mole of reactant, and η is the local overvoltage, which is defined as:

$$\eta = E_0 - E_{ohmic} - E_{cell}. \tag{18}$$

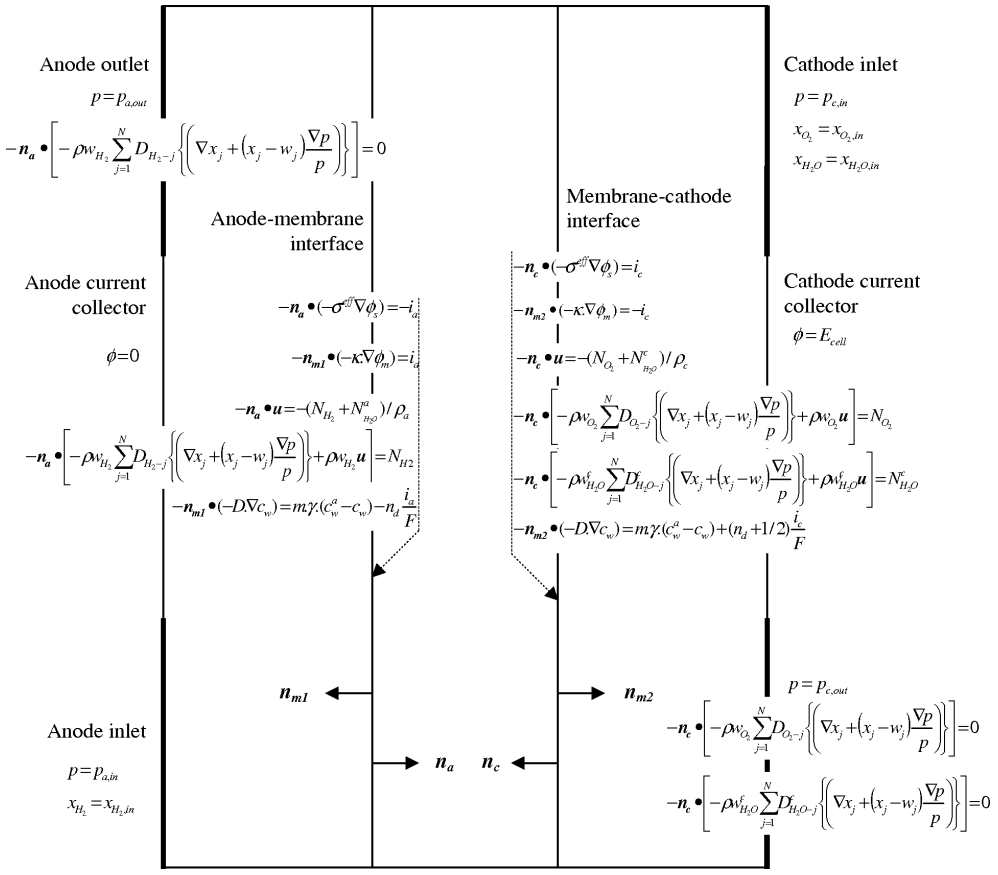

Fig. 3 Boundary conditions used in the model for counter-flow.

In Eq. (18), E_0 is the thermodynamic open circuit voltage, E_{ohmic} is the voltage drop due to membrane resistance, and E_{cell} is the cell voltage. Since the overvoltage is large at the cathode side, the Butler-Volmer equation can be approximated to

$$i_c = i_{0,c}.\frac{c_{O_2}}{c_{O_2 ref}}.\exp\left(\frac{k.F}{R.T}.\eta_c\right), \tag{19}$$

where $c_{O2,\text{ref}}$ is the reference O_2 concentration at 25° C and 1 atm.

At the anode side, with the assumption of constant proton concentration, the transfer current is only dependent on the H_2 concentration and, according to Eq. (17), is given by

$$i_a = k_a.(c_{H_2})^{\gamma_{H2}}\left(\exp\left(\frac{\beta.n.F}{R.T}\eta\right)-\exp\left(-\frac{(1-\beta).n.F}{R.T}\eta\right)\right) \tag{20}$$

The parameters appearing in Eq. (19) and (20) are strongly dependent on the dimensions of the membrane electrode assembly. Therefore, for the cathode, parameters are taken from [8], as these experimental results are used here for validation purposes. Since the model in [8] only concerns the cathode side of the fuel cell, parameters for the anode side are compiled from other sources in the literature, as listed in Table 1.

As the water at the membrane-electrode interface undergoes a phase change, the liquid surface loses its water to the surrounding stream in the porous electrode, which, in turn, results in a concentration jump across the electrode membrane boundary. To implement the jump in water concentration at the interface, the following water uptake mechanisms are used for the anode and the cathode, respectively, as suggested by Berg et al. [17] and Okada et al. [25]:

$$\frac{J^a}{m} = -\gamma\left(c_w - c_w^a\right) \tag{21}$$

$$\frac{J^c}{m} = \gamma\left(c_w - c_w^c\right) \tag{22}$$

Here, the equilibrium sorption values, c_w^a and c_w^c, at the anode and the cathode are the concentrations in the bulk stream, c_w is the surface concentration on the membrane-side, which depends on the activity of water at the associated boundary *via* Henry's Law, and the proportionality constant, γ, is the mass transfer coefficient for water.

The water flux associated with the electro-osmotic drag acts as a sink term at the anode and as a source term at the cathode. By including the flux term for water generated in the reaction, from the mass balance across the interfaces, one can obtain the diffusive flux of water at the anode and cathode side of the membrane as follows:

$$J_{w,a} = -m.\gamma.\left(c_w - c_w^a\right) - n_d\frac{I}{F} \tag{23}$$

Table 4 Geometrical and operational parameters for the base case. [8]

Property	Value
Inlet channel width l_{ch}	0.05 cm
Shoulder width l_{sh}	0.10 cm
Outlet channel width l_{ch}	0.05 cm
Electrode height t_e	0.025 cm
Membrane thickness (Nafion® 115) t_m	0.125 mm
Inlet mol fraction of oxygen $x_{O2,in}$	0.21
Inlet mol fraction of nitrogen $x_{N2,in}$	0.79
Inlet mol fraction of hydrogen $x_{H2,in}$	0.83
Anode and cathode inlet pressure $p_{a,in}$, $p_{c,in}$	1.0133 atm
Anode and cathode outlet pressure $p_{a,out}$, $p_{c,out}$	1 atm

$$J_{w,c} = m.\gamma.(c_w - c_w^c) - (n_d + 1/2)\frac{I}{F}. \quad (24)$$

In Eq. (23) and (24), the local equilibrium value of the water content is calculated as a function of the local water activity, $a = p_{H_2O}/p_{sat}$ as follows:

$$\begin{aligned} c_w^{a,c} &= 0.043 + 17.81a - 39.85a^2 + 36a^3 \quad \text{for } a \le 1 \\ c_w^{a,c} &= 14 + 1.4(a-1) \quad \text{for } 1 < a < 3 \end{aligned}. \quad (25)$$

2.2.3 Current Collectors and Other Boundaries

The potential is set to zero at the anode to specify ground as a reference, and the cell potential is given as the input to the system at the cathode current collector boundary. Zero flux boundary conditions are prescribed for the Maxwell-Stefan equation and Darcy's Law to set zero mass transfer through this boundary. Zero flux boundary conditions are imposed for all equations to exploit symmetries of the system, wherever applicable.

3 Numerical Simulations

The model equations are solved using the commercial computational fluid dynamics package FEMLAB®, which is equipped with a set of predefined partial differential equations, including the Maxwell-Stefan equation, as given in Eq. (3). Along with the direct UMFPACK linear system solver, nonlinear stationary and time dependent solvers are invoked in the simulations. With 3392 triangular mesh elements, the solution becomes satisfactory in the 10^{-4} error tolerance band. There are 21336 degrees of freedom in the discretized domain, which is outlined in Figure 1. The weak formulation of the finite-element method is used for solving the model, where exact Jacobians are generated for the fast convergence of nonlinear models [29]. Using a 2.6 GHz Pentium 4 CPU and 1.5 GB of RAM, the time dependent simulations are completed in about 500 seconds.

4 Results and Discussion

The model used in the simulations is validated with experiments, which were carried out and published by He et al. [8] for an interdigitated PEMFC. Under the assumption that the counter-flow configuration is used, the cell geometry and operational parameters are set to the values reported in [8], including zero humidity at the cathode inlet.

In the absence of transient results, Figure 4 compares the polarization curves from the model and experiments. The polarization curve for the counter-flow case compares reasonably well with the experimental data. Model results indicate that higher voltages are obtained for the co-flow case rather than for the counter-flow case at higher current densities. However, as expected, for lower current densities, in the activation loss region, the two configurations result in the same voltage outputs. The discrepancy between the curves for the co-flow and counter-flow cases in the figure is mainly due to the ohmic loss in the membrane. Essentially, in the co-flow case the membrane is more humidified, and thus, more conductive. Therefore, higher voltages are obtained for the same current drawn from the system, which means that higher current densities are obtained for the same cell voltage.

In the following figures, relating to transient analysis, the plots are intentionally shifted either to the right or to the left for clarity, in all cases the corresponding inputs are given at t = 5 s.

Figure 5 shows the distribution of the water mole fraction at the electrodes and the membrane water content in terms of the water concentration per sulfonic group in the membrane for both counter and co-flow cases. In both cases, fully humidified hydrogen enters the anode and dry air flows into the cathode. According to the figure, the placement of the anode inlet matters for the overall membrane water content. In both cases, the forced flow in the cathode carries water from the reaction sites towards the outlet of the electrode. In the co-flow case, since the anode-side inlet faces the cathode-side inlet, the higher concentration of water on the anode-side is

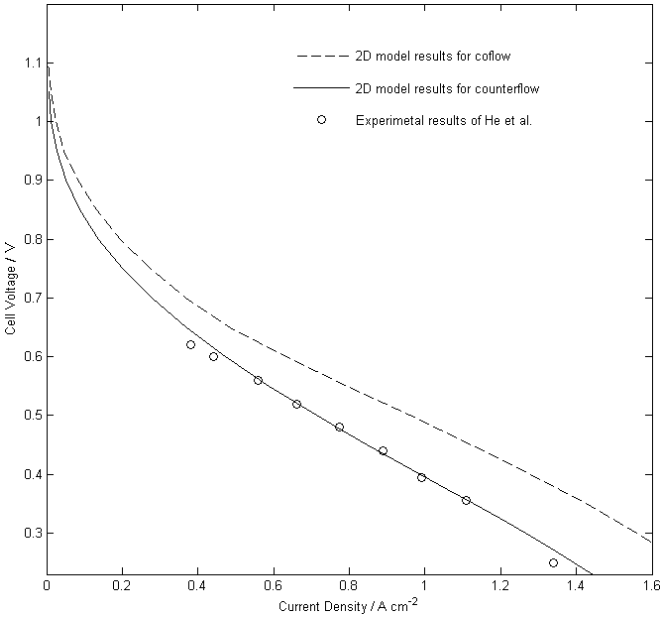

Fig. 4. Comparison of polarization curves for co-flow, counter-flow, and experiment.

carried to the cathode-side by both diffusion and electro-osmotic drag. This results in a higher membrane water content near the inlets. However, in the counter-flow case, since the anode outlet, which is already depleted in water, faces the cathode inlet, the overall membrane water content is greatly reduced. Moreover, water generated during the reaction is partially carried out by the forced flow and partially diffuses into the membrane, resulting in a higher water concentration in the membrane near the outlet than the inlet. This is the reason for the accumulation of water near the outlet of the cathode, especially for the counter-flow case. Consequently, the total current density is expected to be higher near the outlet, compared to near the inlet, as a result of the over-potential distribution, corresponding to ionic transport in the membrane, whose conductivity increases with the water content. However, the oxygen concentration, which also affects the reaction rate (as given in Eq. (19)), is higher near the inlet. These two effects cause the total current density to peak at some central point between the inlet and outlet of the cathode, as shown in Figure 6. It is also clear from Figure 6 that, due to higher water content of the membrane near the anode inlet in the co-flow case, the current density is also significantly higher than in the counter-flow case near the anode outlet as well.

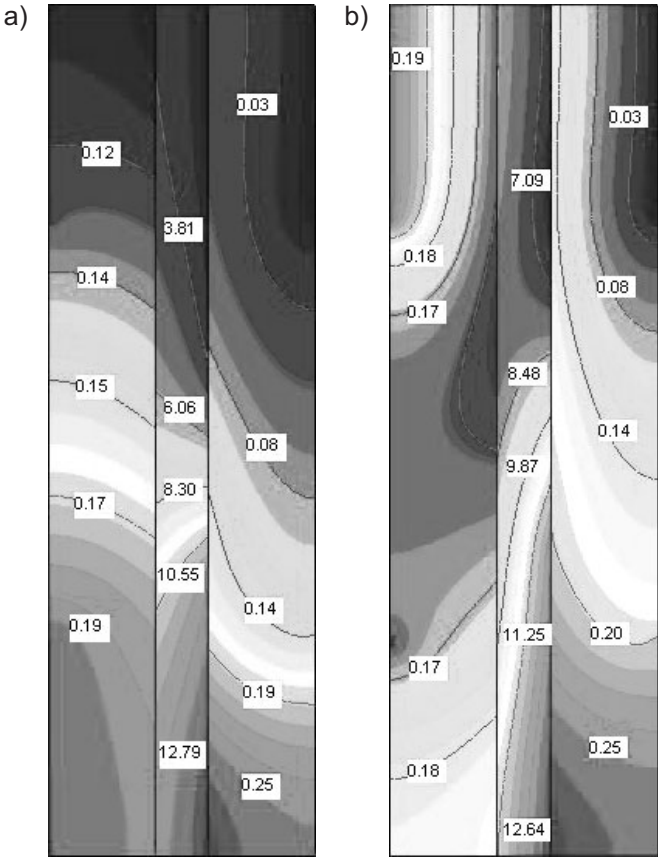

Fig. 5 Surface and contour graphs of water mole fractions at the electrodes and membrane water contents for (a) counter-flow and (b) co-flow. (Color scales are different at different domains of the membrane electrode assembly and can be assessed from the associated contour labels.)

Figure 7 shows the transient response of the average current density to a step change in the cell voltage from 1.1 V to 0.7 V for a dry cathode air inlet, at 1.013 atm. The initial jump shown in the figure is due to instantaneous electrochemical reactions at the specified voltage. After the jump, a 15–20 second transient occurs lasting until the system reaches the steady-state. As pointed out elsewhere, the transient behavior is mainly governed by water transfer through the membrane [6, 10, 11]. The time scale for co-flow is slightly longer than that for counter-flow. This is because, for co-flow more water is accumulated in the membrane than for counter-flow at the same cell voltage, as shown in Figure 5. Therefore, when even more water is coming from the cathode, it takes longer for the

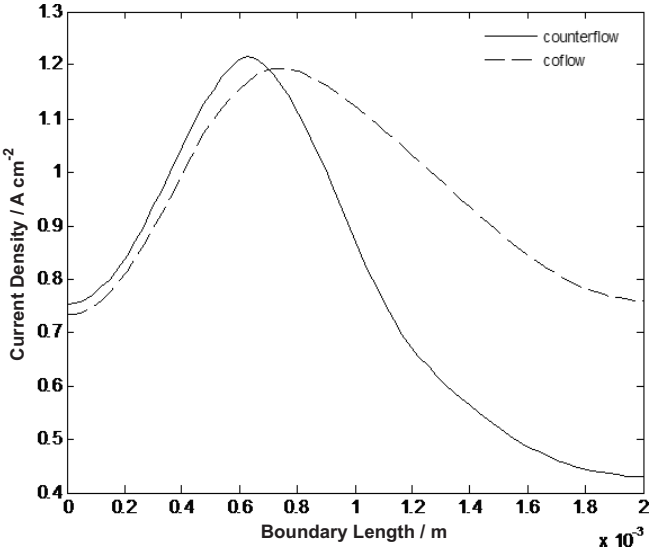

Fig. 6 Distribution of the total current density over the membrane cathode boundary for the co-flow and counter-flow cases from outlet (length = 0) to inlet.

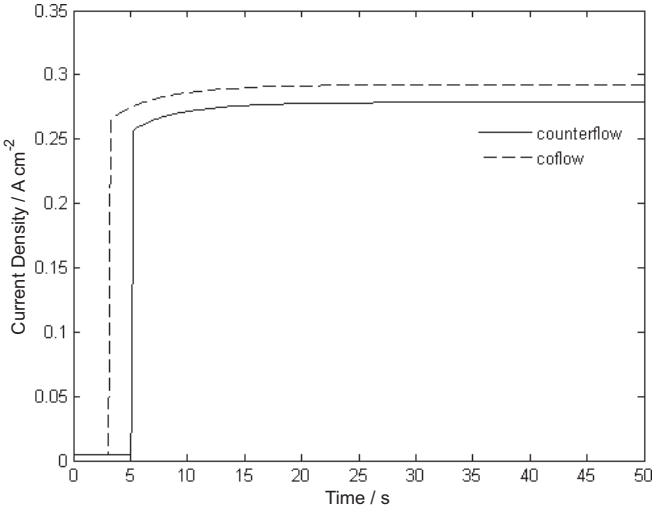

Fig. 7 Step-transient responses of the average current density at start-ups from 1.1 V to 0.7 V with dry cathode inlet air and at 1.013 atm constant pressure for counter-flow and co-flow at $t = 5$ s. (An intentional two-second delay is added to the counter-flow plot for clarity.)

membrane to find a new equilibrium. The diffusive and convective time-scales associated with membrane water transfer are investigated in detail elsewhere [30, 31].

In Figure 8, the transient responses of the average current density for the counter and co-flow cases to simultaneous step changes in the cell voltage from 1.1 V to 0.7 V and the cathode inlet pressure from 1 to 1.013 atms are shown. Overshoots are observed in the average current density response. An increase in pressure from 1 atm to 1.013 atm increases the current density, as reported in the experimental study of He et al. [8]. Therefore, if the pressure is increased at the same time as the voltage decreases, the increase in the current density becomes even more pronounced, resulting in an overshoot. Moreover, overshoots indicate that the reaction rate is boosted for a period of time, and consequently, oxygen in the porous cathode is depleted, in addition to the generation of more water than the steady-state value. In both cases, the transient lasts while the excess water from the reaction diffuses into the membrane. Since the percentage overshoot is larger for the counter-flow case, the transient regime for this case is longer than that of co-flow. The maximum current density values are approximately the same for both flow types. After the transients associated with the water intake of the membrane finish, a different steady-state value is observed for each case.

Figure 9 shows the transient responses of the average current density to step-inputs of both cell voltage and cathode air pressure for counter-flow, simulating system start-up. The effect of the compressor's lag in increasing the air pressure from 1 to 1.013 atm is investigated in three cases: (i) when the voltage input is given in the case where the cathode inlet is already pressurized to 1.013 atm; (ii) when the step voltage input and the cathode inlet pressure are increased simultaneously (pressure to 1.013 atm); and (iii) the pressure is changed 1 second after the voltage input. In all three cases, the current density increases sharply following the voltage drop. Overshoots are observed for cases (ii) and (iii). As the pressure input is introduced at a higher current density, the overshoot observed in the third case is the largest. Due to the overshoots in the second and third cases, the associated settling times are larger than that for the first case. Therefore, it is reasonable to conclude that the pressure must be adjusted prior to increasing the output of the cell at start-up.

Figure 10 shows a failure situation in which the air pressure drops suddenly from 1.013 atm to 1 atm due to a malfunction in the air supply system for a cell operating at 0.7 V. The responses of the average current density for the co-flow and the counter-flow cases are similar. Undershoots of up to 80% are observed in the response of the system for both cases. Following the pressure drop at the inlet, the forced flow in the cathode terminates and the oxygen is depleted in the cathode gas mixture. As shown in the steady-state snapshots at t = 80 s in Figure 11, the water content in the cathode is more than at t = 0. As the membrane water content increases, so does the current density. Furthermore, the times to reach the steady-state values are almost proportional to the depth of the undershoots observed in Figure 10.

Apart from the undershoots in the current density, another undesired occurrence, as a result of the pressure drop, is that water generated in the reaction leaves the cathode from the inlet as well as from the outlet (Figure 11b). Since the pressure difference between the cathode inlet and outlet is lost, there is no transport of species with convection, transport only occurs by diffusion. Therefore, removing the main advantage of the interdigitated PEMFC, the product water cannot be dragged with the shear force of the fluid through the outlet channel. Since dry air enters the cathode, water produced at the membrane boundary diffuses out from the inlet as well as from the outlet. Furthermore, it is reasonable to suggest that increasing the partial pressure of water may result in the condensation and clogging of the pores of the

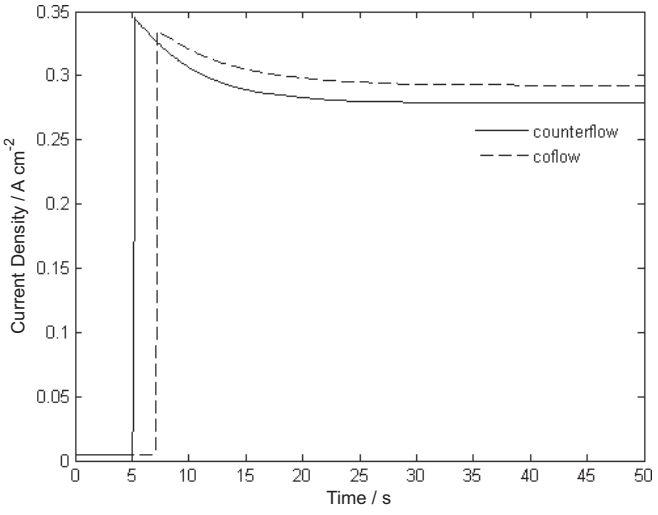

Fig. 8 Step-transient responses of the average current density at start-ups from 1.1 V to 0.7 V with a simultaneous change in air pressure from 1 atm to 1.013 atm with dry cathode inlet air for counter-flow and co-flow at t = 5 s. (A two-second delay is added to the counter-flow plot.)

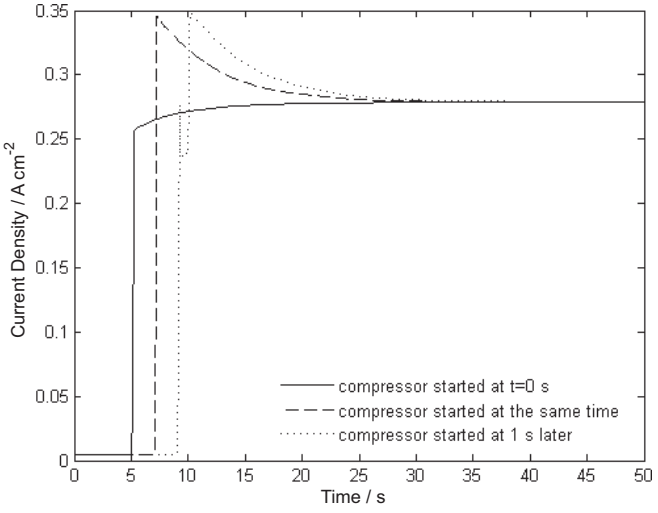

Fig. 9 Comparison of start-ups for counter-flow from 1.1 V to 0.7 V with dry cathode inlet air for pressure inputs applied before the voltage input (—), at the same time as the voltage input (- - - - -), and 1 s after the voltage input (·····). (Two-second delays are placed between plots for clarity.)

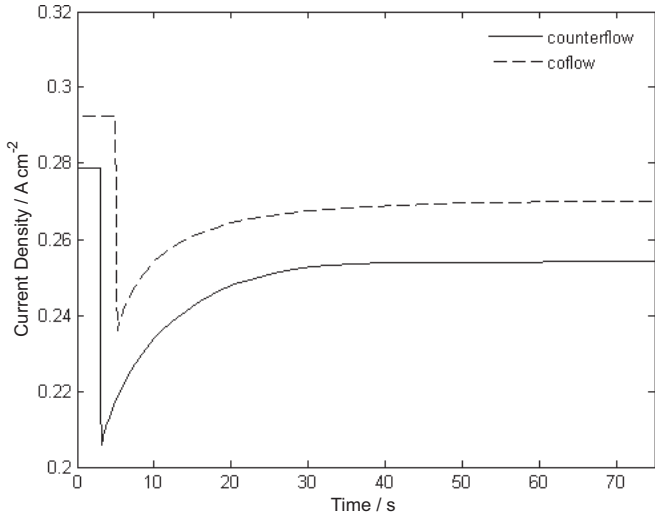

Fig. 10 Dynamic responses of the average current density to a pressure drop from 1.013 atm to 1 atm for 0% humidity at 0.7 V, t = 5 s. (A two-second delay is added to the counter-flow plot.)

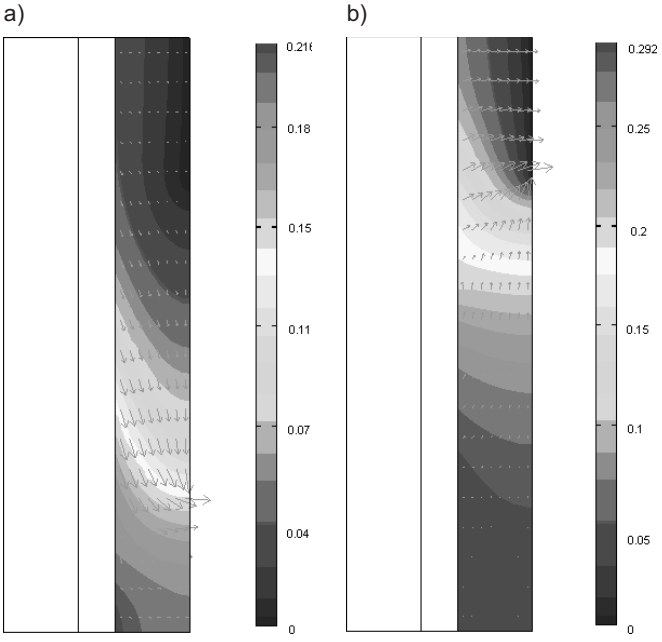

Fig. 11 Distribution of the water mole fraction at the cathode and an arrow plot showing the total flux of water at the cathode for counter-flow at (a) t = 0 s and (b) t = 80 s for the conditions in Figure 10.

cathode by which oxygen molecules are hindered in reaching catalyst sites, resulting in a concentration overvoltage. In order to consider the complete dynamics associated with this phenomenon, the model should include the transport of the liquid phase in the porous electrodes. However, the model results can be interpreted confidently, especially if the activity of water is less than unity.

Figure 12 shows the transients of the average current density for the counter-flow and the co-flow cases in response to a step change in the relative humidity of air from 0.5 to 0 for a cell operating at 0.6 V. This simulation mimics a fault in the humidity control system. It is obvious that the system performance is significantly hindered by the loss in humidity. The current density decreases by almost 35% for co-flow but by only about 25% for counter-flow. Therefore, it is reasonable to conclude that the humidity control system is somewhat more stable for the counter-flow rather than for the co-flow case.

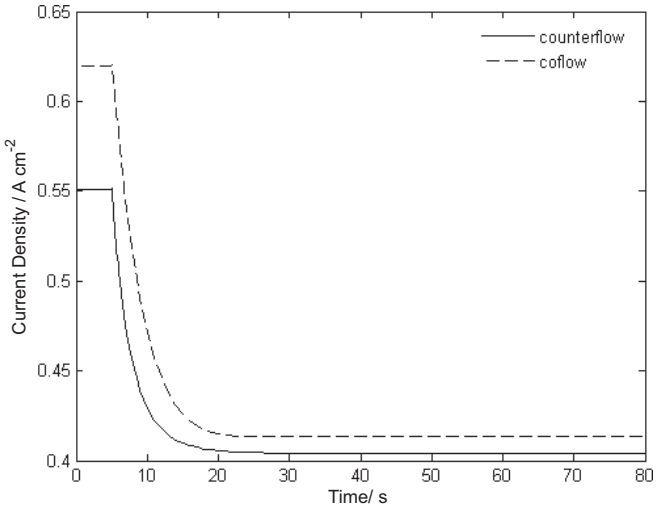

Fig. 12 Transient responses of the average current density to a drop in the relative humidity of the cathode from 0.5 to 0 for 1.05 atm at 0.6 V, t = 5 s.

5 Conclusion

A 2D computational model, including coupled partial differential equations for mass, momentum, and charge conservation inside the membrane electrode assembly of a PEMFC with interdigitated flow fields was developed and used to study the transient responses of the fuel cell system to changes in the cell voltage, pressure, and relative humidity of air for the cases of co-flow and counter-flow. The performances of the co-flow and counter-flow designs were found to be comparable, with a slight advantage for the co-flow design due to somewhat improvement in the membrane water uptake mechanism observed from the transient water profiles each flow type.

Representative transient simulations, regarding the startup schedules of the system, were carried out. It was concluded that, to avoid overshoots and longer transients in the response, the compressor should be turned on initially to provide enough airflow at the cathode, after which the cell could be loaded.

Furthermore, system responses concerning failures in the auxiliary components were discussed. In the presence of a malfunction in the air supply system, such that the inlet channel loses its pressure, up to 80% undershoots were observed from the steady-state response of the average current density. It was also found that, since water transfer is governed by diffusion only, water produced during the reaction also leaves from the cathode inlet. However, it is acknowledged that a detailed study of this scenario calls for a multiphase model. Finally, a failure in the humidity control system is taken into

consideration and a PEMFC employing counter-flow is found to be somewhat less susceptible to failures in this peripheral subsystem.

Finally, it is concluded that the transport of water through the membrane plays the most important role in the transients of a fuel cell system. For the geometry and cases studied here, water transport through the membrane has a time-scale of about 20 to 30 seconds. Detailed work has already been presented for diffusive and convective time-scales [30, 31].

Acknowledgments

Special thanks to Sabanci University for the partial funding of this work under grant number: IACF-04-00221.

References

[1] T. V. Nguyen, *J. Electrochem. Soc.* **1996**, *143*, L103.
[2] W. He, G. Lin, T.V. Nguyen, *AIChE Journal* **2003**, *49 (12)*, 3221.
[3] A. Kazim, H. Liu, P. Forges, *J. Appl. Electrochem.* **1999**, *29*, 1409.
[4] J. S. Yi, T. V. Nguyen, *J. Electrochem. Soc.* **1999**, *146 (1)*, 38.
[5] L. Wang, H. Liu, *J. Power Sources* **2004**, *134*, 185.
[6] M. Hu, A. Gu, M. Wang, X. Zhu, L. Yu, *Energy Conversion Management* **2004**, *45*, 1861.
[7] M. Hu, A. Gu, M. Wang, X. Zhu, L. Yu, *Energy Conversion Management* **2004**, *45*, 1883.
[8] W. He, J.S. Yi, T. V. Nguyen, *AIChE Journal* **2000**, *46 (10)*, 2053.
[9] J. Benziger, E. Chia, J. F. Moxley, I. G. Kevrekidis, *Chem. Eng. Sci.* **2005**, *60*, 1743.
[10] S. Kim, S. Shimpalee, J. W. Van Zee, *J. Power Sources* **2004**, *137*, 43.
[11] W. Friede, S. Rael, B. Davat, *IEEE Transactions on Power Electronics* **2004**, *19 (5)*, 1234.
[12] Y. Wang, C. Y. Wang, *Electrochimica Acta* **2005**, *50*, 1307.
[13] U. Pasaogullari, C.-Y. Wang, *J. Electrochem. Soc.*, **2005**, *152 (2)*, A380.
[14] C. F. Curtiss, R. B. Bird, *Ind. Eng. Chem. Res.* **1999**, *38*, 2515.
[15] J. M. Stockie, K. Promislow, B. R. Wetton, *Int.l J. Numerical Methods In Fluids* **2003**, *41*, 577.
[16] R. B. Bird, W. E. Stewart, E. N. Lightfoot, *Transport Phenomena*, 2nd Ed., Wiley, New York, **2002**.
[17] P. Berg, K. Promislow, J. St. Pierre, J. Stumper, B. Wetton, *J. Electrochem. Soc.* **2004**, *151*, A341.
[18] C. Marr, X. Li, *J. Power Sources* **1999**, *77*, 17.
[19] D. M. Bernardi, M. W. Verbrugge, *AIChE J.* **1991**, *37 (8)*, 1151.
[20] J. L. Fales, N. E. Vandeborough, *Electrochem. Soc. Proceedings* **1986**, *86 (13)*, 179.
[21] B. R. Sivertsen, N. Djilali, *J. Power Sources* **2005**, *141*, 65.
[22] D. M. Bernardi, M. W. Verbrugge, *J. Electrochemical Soc.* **1992**, *139 (9)*, 2477.
[23] T. V. Nguyen, R. V. White, *J. Electrochem. Soc.* **1993**, *140 (8)*, 2178.
[24] T. E. Springer, T. A. Zawodzinski, S. Gottesfeld, *J. Electrochem. Soc.* **1991**, *138 (8)*, 2334.
[25] T. Okada, G. Xie, M. Meeg, *Electrochimica Acta* **1998**, *43*, 2141.
[26] A. C. West, T. F. Fuller, *J. of Applied Electrochem.* **1996**, *26*, 557.
[27] S. Dutta, S. Shimpalee, J. W. Van Zee, *Int. J. of Heat and Mass Transfer* **2001**, *44*, 2029.
[28] C. H. Hamann, A. Hamnett, W. Vielstich, *Electrochemistry*, Wiley-VCH, **1998**.
[29] FEMLAB 3.1 User Guide, COMSOL Inc., Burlington, MA, **2004**.
[30] M. F. Serincan, *MS Thesis*, Sabanci University, **2005**.
[31] M. F. Serincan, S.Yesilyurt in *Proceedings International Hydrogen Energy Congress and Exhibition IHEC 2005, Istanbul, Turkey*, **2005**.

